Soft Nanoscience Letters, 2016, 6, 11-30
Published Online April 2016 in SciRes. http://www.scirp.org/journal/snl
http://dx.doi.org/10.4236/snl.2016.62002

Anisotropy of Photocatalytic Properties in Nanostructured Photocatalysts

Huanchun Wang[1,2], Lina Qiao[1], Haomin Xu[1], Yuanhua Lin[1*], Yang Shen[1], Cewen Nan[1]

[1]State Key Laboratory of New Ceramics and Fine Processing, School of Materials Science and Engineering, Tsinghua University, Beijing, China
[2]High-Tech Institute of Xi'an, Xi'an, China
Email: *linyh@tsinghua.edu.cn

Received 5 February 2016; accepted 15 April 2016; published 18 April 2016

Abstract

Energy band engineering and the nature of surface/interface of a semiconductor play a significant role in searching high efficiency photocatalysts. Actually, the active facets, morphology controlling, especially the exposed facets modulation of photocatalysts during preparation are very desirable. In order to achieve high photocatalytic performance, intrinsic mechanism of such anisotropic properties should be fully considered. In this review, we mainly emphasis on the latest research developments of several extensively investigated photocatalysts and their anisotropic photocatalytic properties, as well as the correlation between effective masses anisotropy and photocatalytic properties. It will be helpful to understand the photocatalytic mechanism and promote rational development of photocatalyst for wide applications.

Keywords

Anisotropy, Carriers, Effective Mass, Photocatalytic Properties

1. Introduction

As one of the most promising approaches for remediating the deterioration of natural environments and utilization of solar energy by the means of splitting water to exploit hydrogen-energy, semiconductor-based photocatalysis has received considerable attention since the landmark work reported by Fujima and Honda in 1972 [1]. Though a great amount of novel photocatalysts and nanostructures were developed to improve the conversion efficiency, it is still far away from practical application and the underlying mechanism in photocatalysis is not thoroughly understood. Generally, a semiconductor photocatalytic redox reaction comprises three steps [2]: il-

*Corresponding author.

How to cite this paper: Wang, H.C., Qiao, L.N., Xu, H.M., Lin, Y.H., Shen, Y. and Nan, C.W. (2016) Anisotropy of Photocatalytic Properties in Nanostructured Photocatalysts. *Soft Nanoscience Letters*, **6**, 11-30.
http://dx.doi.org/10.4236/snl.2016.62002

lumination that induces a transition of electrons from the valence band (VB) to the conduction band (CB), leaving an equal number of vacant sites (holes); migration of excited electrons and holes to the surface; reaction with absorbed electron donors (D) and electron acceptors (A), respectively. Incident light with energy matching the band gap can be absorbed and generate electron-hole pairs. However, many semiconductors with plausible band gap width show poor photocatalytic performance. That's due to the high recombination rate of electrons-holes pairs during the migration which results in few electrons/holes can be found on the surface of photocatalysts. To further improve the photocatalytic performance, a great deal of effort has been paid to reduce or suppress the recombination. Novel nanostructures and composites with heteropical materials are employed, including hierarchical structures, quantum dot decorations, heterostructures with semiconductors and morphology controlling with special facets exposed. Interestingly, morphology controlling over crystal shows superior advantage upon the photocatalytic performance and is regarded as a very efficient approach for advanced properties. Different methods were designed elaborately to fabricate photocatalysts with novel morphologies, especially with particular facets exposed or increasing the proportion of high-energy facets. The underlying facet-dependent mechanisms were proposed and discussed. Though the differences of surface properties are considered to be contributed to the facet-dependent property, including the surface energy, the composition and structure of atoms on the surface, and the defect states, contradictions still exist. With the assistant of theoretical calculation based on density function theory, researchers began to focus their attention upon the properties of charge carriers, which are the most essential mediums during photocatalysis. Amazingly, the charge carriers' properties, in particular the anisotropy of effective masses, show good correlation with anisotropy of photocatalytic performance observed in experiments.

In this review, we will focus on the anisotropy of photocatalytic properties in nanostructured photocatalysts. We begin with the theoretical investigation developments of the carriers' feature in photocatalysts, and the correlation between effective masses' anisotropy and anisotropic photocatalytic properties will be emphatically concerned. The experimental studies of anisotropic photocatalytic properties will be illustrated as a comparison in the following section. Recent progress of tuning the effective masses by modulating the band gap structure will be reviewed in the last section.

2. Anisotropic Properties in Nanostructured Photocatalysts

Anisotropy of photocatalytic properties in nanostructure photocatalysts have been noticed in the form of facet-dependent photocatalytic property and spatial difference over different index photocatalysts crystal facets. Considering that photocatalytic reactions take place on the surfaces of photocatalysts, the exposed crystal facets play a critical role in determining the photocatalytic reactivity and efficiency. Accordingly, the synthesis of single crystals with exposed highly reactive facets has attracted much interest; that is considered to be one of the most promising and efficient avenues for further improvement of photocatalytic performance. However, highly reactive facets usually disappear rapidly during the crystal growth process due to their high surface energy. Base on this point, fabrications of morphology with exposed facets of superior activity need elaborately designed. Several reviews [1]-[9] had summarized the methods of fabricating photocatalysts with peculiar morphology.

Though many photo-responsive materials and photocatalysts exhibit anisotropic performance, and morphology controlling is employed to approach better properties through elaborate experimental techniques, the intrinsic characteristics of anisotropy in photocatalysts are still not thoroughly understood yet. Ye [2] concluded the process of photocatalysis into three steps. The excitation of carriers from maximum valence band to conduction band is supposed to depend on the relativism of band gap width and the wavelength of incident illumination. Due to the quantization of both the band energy and incident light energy, the spatial directivity of electrons' interband transition is negligible. Concerning the third step of photocatalysis, that is the interactions between photo-induced electron-hole pairs and active species absorbed on the surface of photocatalysts, theoretical and experimental investigations revealed facet-dependent characteristics of photo-redox reactions. Proverbially, the differences of these mentioned photocatalytic activities are due to the differences of surface atom structure, surface physicochemical property and work function [10]. However, the transport of charge carriers in the interior of the photocatalysts bulk is another vital factor that affects the efficient of photocatalysis besides surface states. During the transport, partial of carriers recombine at defects sites, exotic atom or impurity band, resulting in the decrease of photocatalytic properties. Most recently, an increasing number of research focuses on the transport characteristic of carriers, especially the intrinsic features of carriers, including the effective masses along differ-

ent crystal orientation.

2.1. Anisotropy of Carriers' Effective Mass

As is known, the effective mass of electron/hole is a tensor in semiconductor. It is considered as a quantity responding to a periodic potential in crystal field and is used to describe the band structures of photocatalysts. Usually, the effective mass can be calculated by the following equation:

$$m^* = \pm\left(h/2\pi\right)^2\left(\mathrm{d}^2E/\mathrm{d}k^2\right)^{-2}$$

where m^* is the efficient mass, h is the Planck constant, k is the wave vector, E is the energy of wave vector k. It is clear that the electron and hole in the flat level with constant gradient have higher efficient masses, and contrarily those in bent level with variable gradient have lower efficient masses. Due to the difference of band structures, effective masses located at different spot in reciprocal space behave different from each other. The effective mass of carrier in semiconductor is supposed to be closely correlated to the transport property and dominate the mobility of carriers. The smaller effective mass is, the better the mobility is, which makes carrier transport to the surface much more straightforward, and decreases the probability of recombination [11]. On the contrary, the larger efficient mass results in the worse mobility. A complex understanding of carriers' property will be conducive to a deeper insight of photocatalysis process and developing more efficient photocatalysts.

Ye comparatively investigated the effective mass of Ag_2O, Ag_3PO_4 and $AgNbO_3$ using first-principles calculations based on the density functional theory [12]. The calculation results released that the conduction band minimum (CBM) of Ag_3PO_4 mainly consists of Ag *s* states, while Ag *d* states predominate the CBM in Ag_2O and $AgNbO_3$ (**Figure 1**). Due to the dispersive character of *s* state, the wave function in Ag_3PO_4 is highly delocalized. It reflects in the effective mass of electrons in Ag_3PO_4. With the hybridization of *s* state located at the bottom of conduction band, the effective mass of electrons is smaller in Ag_3PO_4 than that in the other two photocatalysts in every direction (**Table 1**). In contrast, the CBM consists mainly of d_{xz} and d_{yz} in $AgNbO_3$, which leads to an anisotropic charge distribution. This anisotropy character allows electrons transfer only along the *z* direction, indicating that the $AgNbO_3$ {001} surface is especially active for reduction reactions. The calculated effective masses of electrons also show that it is much smaller in {001} direction than in other two directions. Furthermore, the anisotropy of band structure also reflects in the valence band maximum (VBM) and the effective mass of holes. The VBM of Ag_3PO_4 and $AgNbO_3$ were mainly predominated by Ag *d* state (**Figure 1**). Due to the steric configuration of *d* orbit, the charge density is selective distributing along particular direction. The calculation results indicate that the effective masses of holes absolutely depend on the crystal orientation. Though the photocatalysts are used in the forms of powder in most case, and the selective nature of the reactive facet is suspected to be disadvantageous for photocatalysis. Theoretical prediction of the correlation between effective masses of carriers and the photocatalytic activities is consistent well with the experimental results [11] for Ag_3PO_4. As for Ag_2O, the effective mass of electrons along {100}, {110} and {111} directions are almost the same ($0.61m_e$), while the weighted average of the three degenerate holes along three directions are calculated to be 2.038 m_e, 1.855 m_e and 1.621 m_e, respectively. The different value of the weighted average of the effective mass of a hole distinguish the mobility of the photogenerated electrons and holes, causing the lower recombination rate of the e^--h^+ pairs and resulting in the higher photocatalytic activity [13].

Table 1. Effective masses of the electron (m_e^*) and the hole (m_h^*) for Ag_3PO_4 obtained from parabolic fitting to the CBM and the VBM along each direction in the reciprocal space, respectively. Reproduced with permission [12], copyright 2011, The American Physical Society.

Orientation	m_e^*/m_0			m_h^*/m_0		
	100	110	111	100	110	111
Ag_2O	0.61	0.61	0.62	2.06	2.09	1.82
Ag_3PO_4	0.41	0.42	0.43	3.04	2.56	1.99
$AgNbO_3$	0.79	7.60	3.45	4.77	3.81	3.92

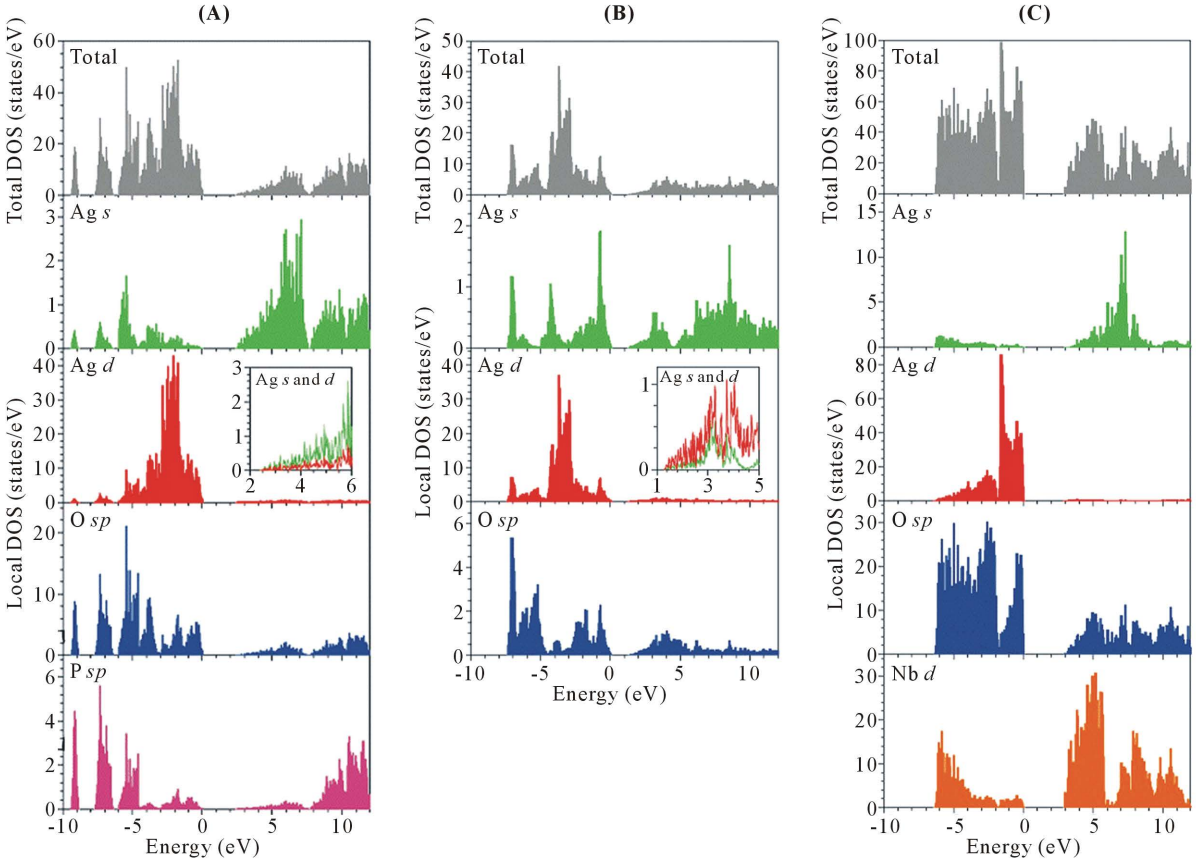

Figure 1. Total and local DOS for (A) Ag_3PO_4, (B) Ag_2O and (C) $AgNbO_3$. The zero energy is at the VBM. The insets in local DOS in (A) and (B) show extended plots of DOS for Ag *s* and *d* at the energy range near the CBM. Adapted with permission [12], copyright 2011, The American Physical Society.

Recently, theoretical investigations of effective masses of carriers were carried out to get a deeper insight of anisotropy over other photocatalysts. It was revealed that a reasonable combination of different surface in a single crystal leads to superior photocatalytic activity than that of crystal with only one component exposed facet. It was assume to be attributed to the preferential flow of carriers along special direction. However, the underlying reasons remain far from whole understanding.

Titanium dioxide (TiO_2) is one of the most extensively investigated photocatalysts due to eco-friendly nature, physicochemistry stability and convenient fabrication technology. The facet dependent performance of TiO_2 stimulated intense interest of its intrinsic feature. Huang [14] examined the trapping energies of photogenerated holes and electrons in TiO_2 on the basis of density functional electronic structure calculations. Their results leaded to a conflicting order of relative photooxidation and photoreduction activities of different facets with conventional understanding. By defined the trapping energy as composed of the energy gained by placing the hole in a localized oxygen *p* orbital and the lattice distortion energy expended to accommodate the polaron, {101} facets show the highest trapping energy for both electrons and holes. Meanwhile, as the difference in trapping energy between the {100} and bulk, a large driving force of holes along the {100} direction is supposed (**Figure 2(A)**). In the same way, the electrons is expected to transfer along {101} direction. That leads to the spatial separation of photo-induced electrons and holes on {101} and {100} facets [15].

On the other hand, such an intrinsic anisotropic transport property in TiO_2 crystal can be explained from another perspective: the anisotropy of effective masses of carriers. Although anatase TiO_2 shows lower absorbance ability than rutile and brookite due to the larger band gap (3.2 eV) than that of rutile (3.0 eV), anatase possess obviously superior photocatalytic activities to that of the other allotropies in degradation of organic dyes and water splitting. Yu [16] investigated the electronic structures and effective mass of anatase, rutile and brookite TiO_2 by first-principles density functional theory (DFT). The constitutions of DOS in anatase, rutile and

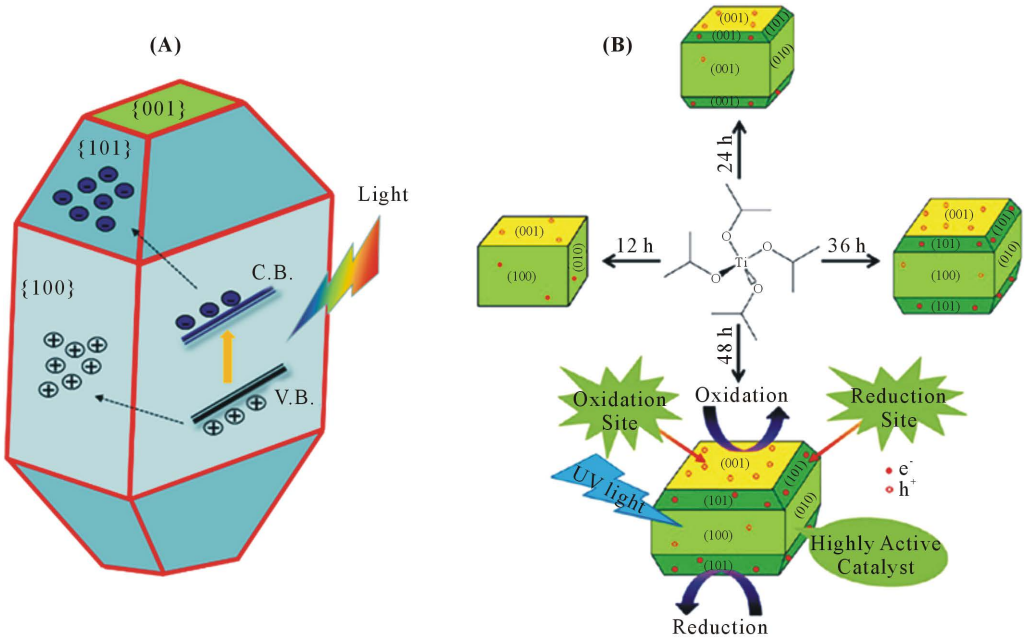

Figure 2. (A) Schematic representation of the spatial accumulation of photogenerated electrons and holes directly on {101} and {100} facets, respectively over TiO_2 nanoparticles. (B) Schematic of TiO_2 NCs with different exposed facets in the hydrothermal reaction duration, and the redox sites on different exposed facets. Adapted with permission [15], copyright 2013, American Chemical Society.

brookite are similar. The valence bands primarily consist of O 2*p* states and a few Ti 3*d* states, and the conduction bands are mainly composed by Ti 3*d* states, mixed with a few O 2*p* and Ti 3*p* states. However, the calculated average effective mass of electrons and holes in anatase is smaller than that in rutile and brookite. Generally, the transfer rate of photogenerated carriers is inversely proportional to their effective masses; the small effective mass of photogenerated carriers promote the migration and inhibit the recombination of charge carriers, resulting in enhanced photocatalytic activity. In view of this point, the theoretical results fit well with the actual situation. Moreover, the anisotropy of effective masses of electrons and holes was also revealed. Similar method was also employed in calculating the effective mass of carriers for silver halide-based Ag@AgX (X = Cl, Br, I) [17], $CaZrTi_2O_7$ [18] and $BiVO_4$ [19] to illustrate the photocatalytic property. Calculations showed the valence band (VB) and conduction band (CB) of $BiVO_4$ mainly consist of O 2*p* states, V 3*d* states, and Bi 6*p* states. The Bi 6*s* states also contribute to the composition of upper VB. Due to the hybridization states between Bi 6*p* states, O 2*p* states and V 3*d* states, and the splitting of V 3*d* in the tetrahedron crystal field effect, the chemical bonding exhibit spatial directional features. This feature reflects in the effective masses of carriers along different direction in Brillouin zone of monoclinic clinobisvanite (**Figure 3**). That indicates the anisotropic effective masses of carriers along different crystal orientation and preferential photocatalytic property.

A more in-depth calculation and comparison were carried out for AgX (X = Cl, Br, I) [17]. The effective masses of holes (m_h^*) and electrons (m_e^*) along various directions were calculated by fitting parabolic functions to the CBM and VBM of silver halides. The calculation results demonstrated that m_e^* is small and almost equivalent along every direction. As the anion of the silver halide changes from chlorine to iodine, the effective masses of electrons decrease from ~0.25 m_e to ~0.18 m_e, ~0.15 m_e and ~0.13 m_e for AgCl, AgBr, AgI (W), and AgI (ZB), respectively. However, the properties of holes inhibit a various tends among AgX. The effective masses of holes along the {100} direction are considerably larger than those along the {110} and {111} directions for AgCl and AgBr, and {111} direction possess the smallest effective masses. Nevertheless, the picture reverses for AgI. As for AgI (ZB), the effective masses of holes along {100} direction is much smaller than that along {110} and {111}, and is smaller than that in AgCl and AgBr along {111} directions. It indicates that the {110} and {111} surfaces of AgCl and AgBr show higher photocatalytic activities than the {100} surfaces, while the {100} surfaces of AgI (ZB) show higher activities than the {110} and {111} surfaces due to the preferential transport of holes. Furthermore, the aforementioned anisotropy of holes' effective masses could be explained by

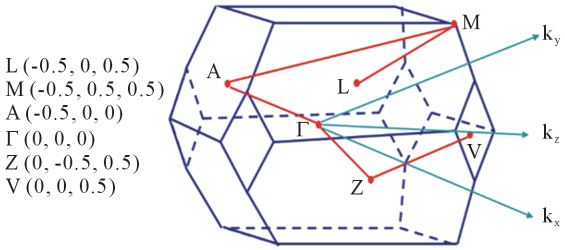

	Band gap/eV	m_{h^*}/m_0	m_{e^*}/m_0
L→L	2.243		
VBM→CBM	2.174	1.04(L→M)	3.557(L→M)
M→M	3.007		
MA_1→MA_2	2.517	1.195(A→M)	0.962(A→M)
A→A	2.245	0.726(A→M)	0.898(A→M)
Γ→Γ	2.803	0.894(Γ→Z)	5.602(Γ→A)
Z→Z	2.243	3.038(Z→Γ)	0.896(Z→Γ)
ZV_1→Z	2.202	2.675(V→Z)	
V→V	3.006		

Figure 3. The Brillouin zone of monoclinic clinobisvanite $BiVO_4$ in the reciprocal lattice. The selected k-point path (red line) and the calculated band gaps the corresponding effective mass of carriers between different k-points. Reproduced with permission [19], copyright 2011, The Royal Society of Chemistry.

the character of valence band in AgX. The valence band is supposed to consist of Ag 4*d* and *p* orbit of halogen. However, the Ag 4*d* orbitals are splitting into t_{2g} and e_g states causing by octahedral crystal field in AgCl and AgBr or tetrahedral crystal field in AgI (W) and AgI (ZB). The e_g states are composed of d_z^2 and $d_{x^2-y^2}^2$ orbital, while The t_{2g} states are composed of d_{xy}, d_{yz}, and d_{xz} orbital, both of which show an anisotropic charge distribution, therefore leading to a different effective mass of holes along different directions. Moreover, *p* orbitals states are much dispersive than the localized *d* orbitals. As the anion of the silver halide changes from chlorine to iodine, the component of *p* orbitals in conduction band increases due to the increase of atomic radius, and smaller effective massed can be expected. The density of states (DOS) near Fermi levels confirmed the prediction and indicated that increased halogen *p* states in the upper valence band would enhance the dispersiveness of the upper valance band, thus a smaller effective mass can be obtained.

Such anisotropies of carriers effective masses were also reported in $ZnGa_2O_4$ [20] and $Cu_2(OH)PO_4$ [21]. Based on the effective mass theoretical investigation above, superior mobility along specific direction and higher photocatalytic activity on specific exposed facets can be predicted in compared with those directions and facets with inferior transport features.

Though the facets-dependent photocatalytic performance of nanostructured photocatalysts was elaborated theoretically as to be attributed by the difference of surface properties, practical situation seems more complex and contradictory opinion arise. Alternatively, the anisotropy of carriers' effective masses and anisotropic photocatalytic performance show interesting correlations, and seem to be consistent well.

2.2. Anisotropic Photocatalytic Performance

2.2.1. Ag-Based Photocatalysts

Ag_3PO_4 is a novel visible light responsible photocatalyst with indirect band gap of 2.36 eV. Due to its high quantum yield and excellent performance in photodegradation of organic dyes, different morphologies and regular nanostructures with varying exposed facets have been synthesized through novel approaches. Bi [22] [23] synthesized Ag_3PO_4 sub-microcubes through a complex-precipitation strategy by reacting $[Ag(NH_3)_2]^+$ with Na_2HPO_4 at room temperature. After tailoring the morphology and structure through adjusting synthetic parameters, they found cubic crystals with their surface dominated by (100) planes exhibited much higher catalytic activities and photoelectric properties than spherical particles under visible-light irradiation (**Figure 4(A)**). Furthermore, reported by the same group, single-crystalline rhombic dodecahedrons Ag_3PO_4 can be facile fabricated using CH_3COOAg as precursor, and exhibit superior photocatalytic properties in comparison with cubes for the degradation of organic contaminants (**Figure 4(B)** and **Figure 4(C)**) [24].

In view of the anisotropy of photocatalytic activities on {110} and {100}, more subsequent experimental work focused on fabrication of novel Ag_3PO_4 with increased {110} exposed facet. Wang [25] synthesized tetrapod shaped Ag_3PO_4 through a facile precipitation route without surfactant from a reaction of silver-amino ($[Ag(NH_3)_2]^+$) complex and Na_2HPO_4 in aqueous solution. The selectively absorb of Na_2HPO_4 plays an essential role in forming Ag_3PO_4 tetrapods. However, using urea instead of NH_3 leads to similar results [26]. Urea decompose into NH_3 in hydrothermal process and refluxing system, and will selectively absorb on the {111} planes, resulting in the restrained growth of {111} planes. Through this dynamic control, {110} facets-dominated tetrapod with higher activities than polyhedrons was obtained (**Figure 4(D)**). The superior performance of {110} facets-dominated

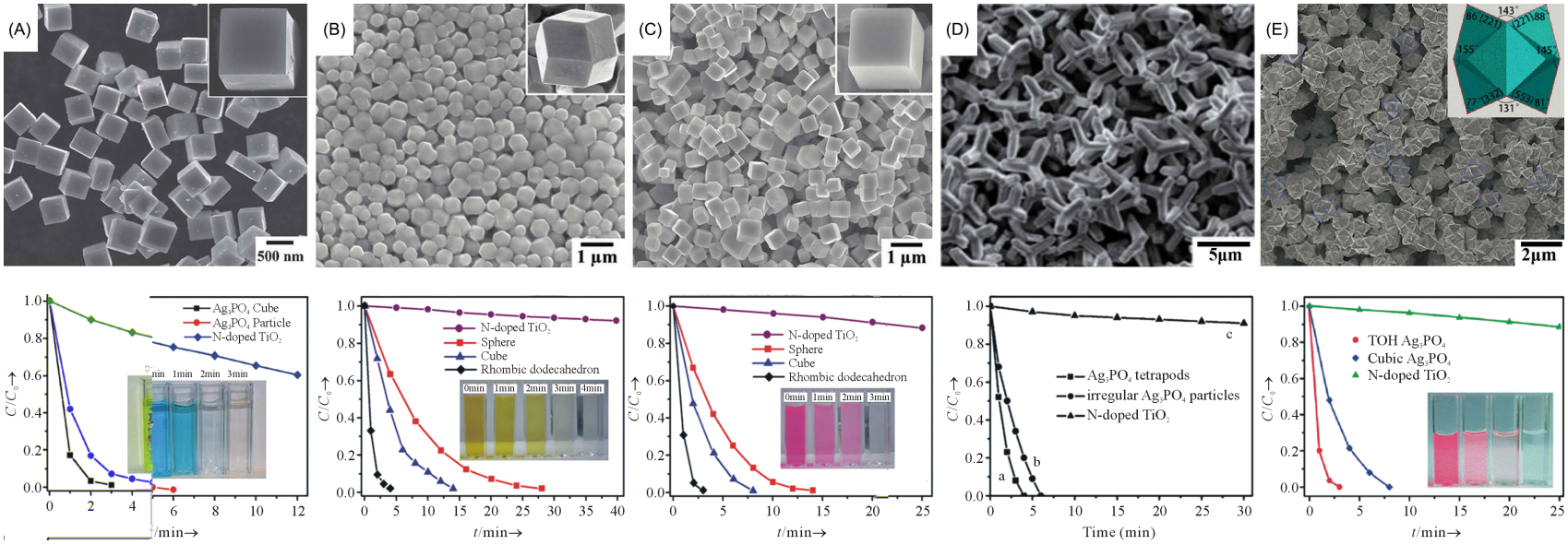

Figure 4. The SEM images of Ag_3PO_4 with morphologies of (A) sub-microcubes; (B) rhombic dodecahedrons; (C) sub-microcrystals cubes; (D) tetrapods; (E) concave trisoctahedron; and corresponding photocatalytic activity comparison of Ag_3PO_4 sub-microcrystals in degradation of dyes under visible light illumination. (A) and (E) Reproduced with permission [22] [27]. Copyright 2012/2013, The Royal Society of Chemistry; (B) and (C) reproduced with permission [24], copyright 2011, American Chemical Society. (D) Reproduced with permission [25]. Copyright 2012, The Royal Society of Chemistry.

tetrapod can be predicted by the smaller effective mass of hole (m_h^*) along {110} orientation. Despite that the effective mass of hole along {111} orientation is the smallest, such high-index facets degenerate during the growth process because of their high surface energies. Using Au@Ag core-shell nanorods (NRs) as starting materials based on the heteroepitaxial growth procedure, Jiao synthesized concave trisoctahedral with high index facets Ag_3PO_4 [27]. Although owning much larger dimensions and smaller surface area than cubes, concave trisoctahedral Ag_3PO_4 microcrystals exhibited higher photocatalytic activity than cubic submicro-crystals (**Figure 4(E)**). That is significant different from the mechanism that mainly attributed to their surface areas.

Except silver orthophosphate, other Ag-based compounds also demonstrate anisotropic photocatalytic properties. Silver (I) oxide (Ag_2O), with a narrow band gap of 1.3 eV, was usually used as co-photocatalyst because of their instability under light irradiation. Wang [13] synthesized five morphologies of Ag_2O microcrystals (cubic, octahedral, rhombic dodecahedra, polyhedra with 18 faces and rhombicuboctahedral) through kinetic control by using complexing agents (**Figure 5**). By photodeposition of Ag on the surface of Ag_2O microcrystal, anisotropic photocatalytic activities for degradation of methyl orange (MO) under visible light irradiation were noticed. With the increase of exposed {100} facets, the photocatalytic properties were gradually strengthened from rhombicuboctahedral to polyhedra with 18 faces. Cubic Ag@Ag_2O with exposed {100} facets showed the

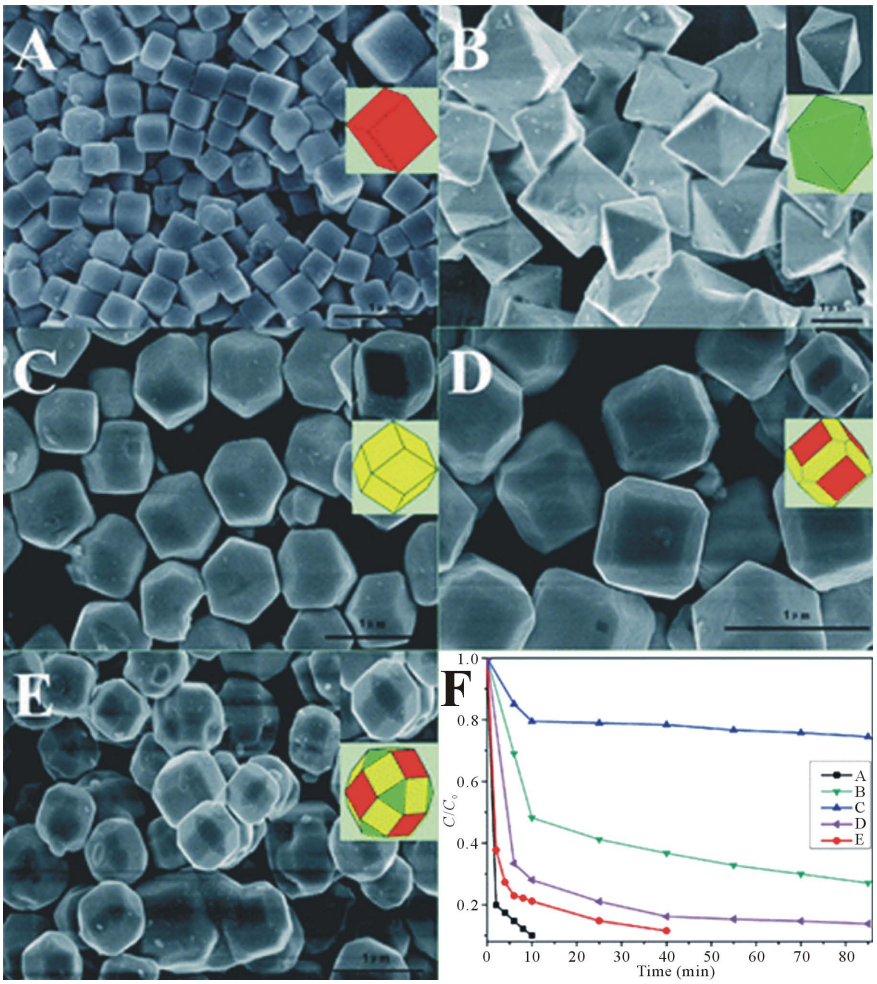

Figure 5. SEM images of the Ag_2O microcrystals synthesized with various morphologies: (A) cubes with exposed {100} facets, (B) octahedra with exposed {111} facets, (C) rhombic dodecahedra with exposed {110} facets, (D) polyhedra with 18 faces with exposed {100} and {110} facets, (E) rhombicuboctahedral with exposed {100}, {110} and {111} facets, (F) corresponding photocatalytic activities comparison of Ag@Ag_2O with different exposed facets. Adapted with permission [13], copyright 2012, Royal Society of Chemistry.

highest activity of all the other morphologies. 90% of degradation rate of samples was achieved in 10 min (**Figure 5(F)**).

Silver halide AgX (X = Cl, Br, I) is another category Ag-based photocatalysts which has attracted increasing attention recently [17] [28]-[31] because of its suitable band-gap width and it can precipitate Ag nanoparticles through in-situ photoreduction under irradiation. Metallic Ag nanoparticles will enhance the photoresponse due to the plasmonic effect and stability of these AgX-based photocatalysts. However, photocatalysis on these series compounds is facet-dependent and even show distinct reaction behaviors on different facets spatially. Several approaches are attempted to controlling the morphology and improving the photocatalytic property. Kuang [32] synthesized wurtzite-type β-AgI (the most stable phase below 420 K) platelet microcrystals with polar {0001} facets by precipitation reaction with the assistant of polyvinylpyrrolidone. On the Ag^+-terminated (0001) faces, the surface lattice Ag^+ ions is reduced by the photogenerated electrons which results in the formation of Ag metal, while the photogenerated holes will oxidize the surface lattice I^- ions to highly volatile I_2, leaving lots of pinholes on the I^--terminated {0001} faces. Zhang [30] reported for the first time the synthesis of trapezohedral (TPH) and concave hexoctahedral (HOH) AgCl nanocrystals (NCs) by direct solvothermal method with the assistant of a specific ionic liquid poly (diallyldimethylammonium) chloride (PDDA), which acts as Cl ion precursor and a morphology controlled stabilizer (**Figure 6(A)-(D)**). These unconventional polyhedral, enclosed by 24 high-index {311} facets and 48 high-index {15 5 2} facets, exhibits much higher photocatalytic activity for the degradation of organics under sunlight than octahedral AgCl NCs which have mainly {111} faces exposed, though the former has lower surface areas and surface energies.

Morphology control and facet-dependent photocatalytic property of AgBr were studied by Guo's Group [28]. Three types of AgBr nanocrystals, evolved from cubes through truncated cubes and finally octahedra, were synthesized through controlling the reaction temperature and the amount of added polyvinylpyrrolidone (PVP) (**Figure 6(E)-(H)**). According to the XRD results, cube AgBr nanocrystals were bounded by six {100} facets, while octahedra nanocrystals were enclosed by eight {111} facets. More importantly, the {111}-dominated octahedral showed the highest photocatalytic activities. Similar phenomenons were also observed over AgBrnanoplates [29] or polyhedral microcrystals [31] with exposed {111} facets constituted by Ag atoms obtained by ion-exchange process. Due to the superior activity of {111} faceted AgBr, polyhedral AgBr/Ag microcrystals were also fabricated integrating efficient plasmonic effect to photocatalysts with increasing percentage of exposed high-reactivity AgBr {111} facets [31]. Apparently, morphology control based on the anisotropy of photocatalytic activity has drawn much attention and is proved to be an effective way to improving AgX-based photocatalysts.

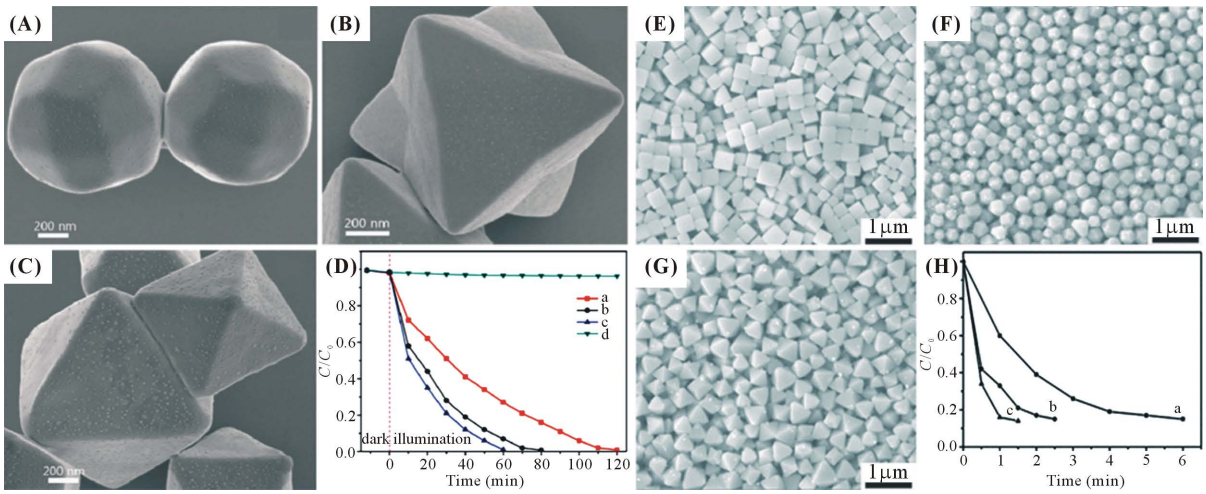

Figure 6. SEM images of different AgCl NCs after photodegradation experiments: (A) trapezohedral (TPH), (B) concave hexoctahedral and (C) octahedral; (D) The corresponding comparison of MO dye photodegradation dynamics under visible light irradiation (A) octahedral AgCl NCs, (B) TPH AgCl NCs and (C) concave HOH AgCl NCs, and (D) without a catalyst. Adapted with permission [30]. Copyright 2015, The Royal Society of Chemistry; SEM images of as-prepared AgBr polyhedral, (E) cubes, (F) truncated cubes, (G) octahedra, and (H) the corresponding photodegradation of MO dye over them. Adapted with permission [28], copyright 2012, John Wiley and Sons.

2.2.2. Bismuth-Based Photocatalysts

Bismuth-based compounds are novel photocatalysts which have attracted extensive interest in the last few decades due to the promising visible-light responsive photocatalytic performances resulting from unique energy band structure and appropriate band gap width. However, anisotropic photocatalytic property was also concerned over several bismuth-based photocatalysts, and morphology control was employed to hunt for more satisfactory photocatalytic property. Li's Group [33]-[36] carried out series of experiments about the facet-dependent property of $BiVO_4$. Monoclinic $BiVO_4$ crystals with preferentially exposed {040} facets were hydrothermally synthesized by using a trace amount of $TiCl_3$ as the directing agent at suitable pH value [37]. By comparative studying of the oxygen evolution rate with different {040}/{110} ratio, they found that the photocatalytic water oxidation activity of $BiVO_4$ correlated very well with the extent of exposure of the {040} facet. With almost the same hydrophilicity and surface area, the {040} facet was assumed to provide multi-atomic BiV4 center as active sites. Nevertheless, more complicated mechanism and photocatalytic behavior were revealed in subsequent experiments.

Using monoclinic bismuth vanadate crystal as a model photocatalyst, efficient separation of photogenrated electrons and holes can be achieved on different crystal facets which are adjacent instead of along with direction of crystal built-in electric field. Considering the facet-selective photo-deposition of metals and oxides, which are oxidizing reaction and reduction reaction, respectively, the existence of oxidation and reduction facets were confirmed (**Figure 7**) by Li's Group [33] [34]. However, the reason that the photo-induced electrons and holes migrate to special facets was assumed to be mainly owing to the difference of energy levels of these facets.

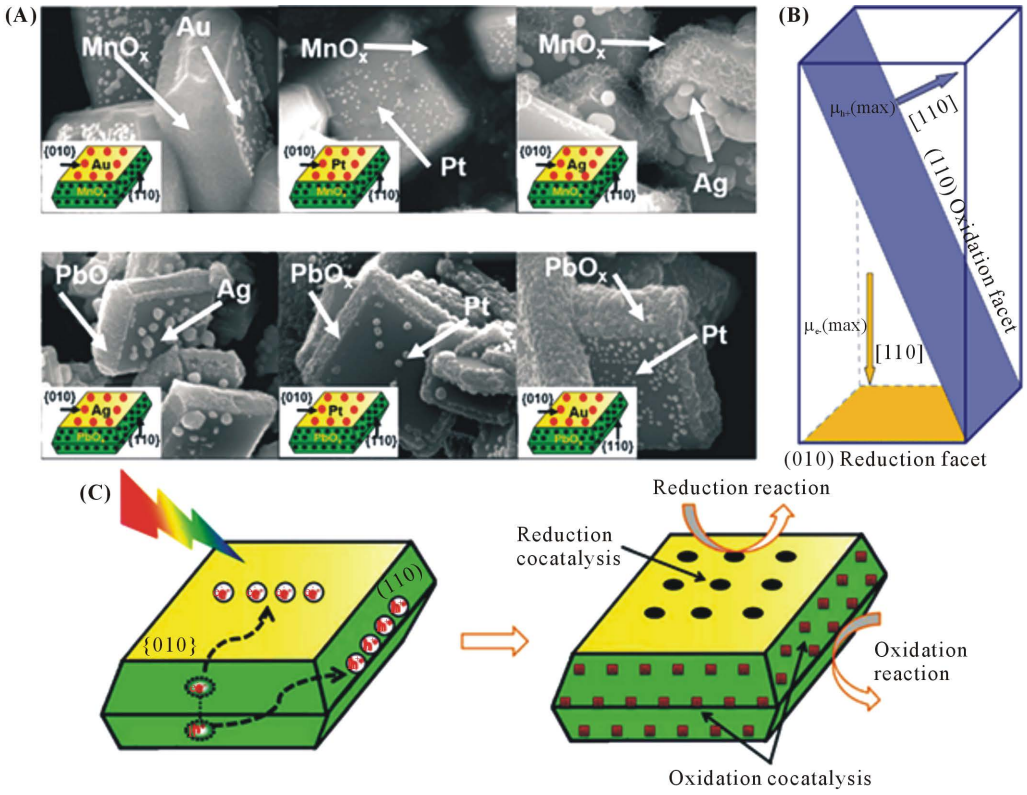

Figure 7. (A) SEM images of selectively photo-deposited metal oxides and noble metals on different $BiVO_4$ monocrystal surface. Redox reaction of metal precursors and photodeposition of metal oxides and noble metals on adjacent facets are used to illustrate the anisotropic photochemical activity of $BiVO_4$ monocrystal. Reproduced with permission [33], copyright 2013, Nature Publishing Group. (B) The scheme of electrons and holes transfer paths along the crystal axis [hkl] and the corresponding facet (hkl) in $BiVO_4$ crystal. Reproduced with permission [35], copyright Bi *et al.* 2015, The Royal Society of Chemistry. (C) The scheme of selective deposition of reduction and oxidation co-catalysts on {010} and {110} facets of $BiVO_4$ based on the charge separation between different facets. Adapted with permission [34], copyright Bi *et al.* 2014, Royal Society of Chemistry.

Besides indirect chemical approaches, including photo deposition and photoelectrochemical water oxidation reaction, to distinguish the spatial separation of the photogenerated electrons and holes, direct imaging of highly anisotropic photogenerated charge separations and theoretical study using density functional theory [35] [36] were employed. Highly anisotropic photoinducedhole distribution is observed for single $BiVO_4$ crystals by combining the KPFM and transient SPV techniques (**Figure 8**) by the same group [36]. The enhanced built-in electric field caused by the surface band bending in the SCR between {011} facet and {010} facet was proposed to responsible for the anisotropy.

However, not considering the surface factor, for example, surface band bending, surface energetic differences, etc., anisotropy was still certified by theoretical prediction [35]. Due to the highly stability resulting from low surface energy, {010} and {110} facets are highly exposed. Alternatively, electrons prefer to transfer along {010} direction and holes transfer along {110} direction because of the largest mobility of electrons and holes in the preferential direction. That comes to an intuitional impress that the anisotropy of photocatalysis should be intrinsic character of crystal and not be determined by surface property. Of course, surface factors of crystal have affected photocatalysis process by interaction with species which involved in redox reaction. Analogous regulations were reported by other groups [38] [39].

Not surprisingly, anisotropic photocatalytic performance is universal phenomenon in layered structure bismuth-based photocatalyst, especially BiOX (X = Cl, Br and I). All BiOX have a tetragonal matlockite structure, a layer structure characterized by $[Bi_2O_2]$ slabs interleaved by double slabs of halogen atoms along with c axle. Normally, {001} facets are thermodynamic favorable because of low surface energy.

BiOCl single-crystalline nanosheets with exposed {001} and {010} facets can be selectively synthesized via hydrothermal route by adjusting pH value [40] (**Figure 9**). The as-prepared BiOCl nanosheets with exposed {001} facets exhibited higher activity for direct photoexcitation pollutant degradation under UV light than that exposed with {010} facets. Unexpected, BiOCl with exposed {010} facets possessed superior activity for indirect dye photosensitization degradation under visible light. The results suggested that different crystal facets possess various light-dependent photocatalytic properties, though different mechanism is involved. However, on account of the superior capacity in direct photocatalytic degradation of organic pollutant, special synthetic methods are employed to prepare {001} facets exposed in a high percentage for superior photocatalytic property. Using organic metal salt, BiOCl nanosheets with tunable {001} facets percentages can be fabricated [41]. By comparing the photo-degradation efficiency of RhB on different percentages of the {001} faceted BiOCl, it was

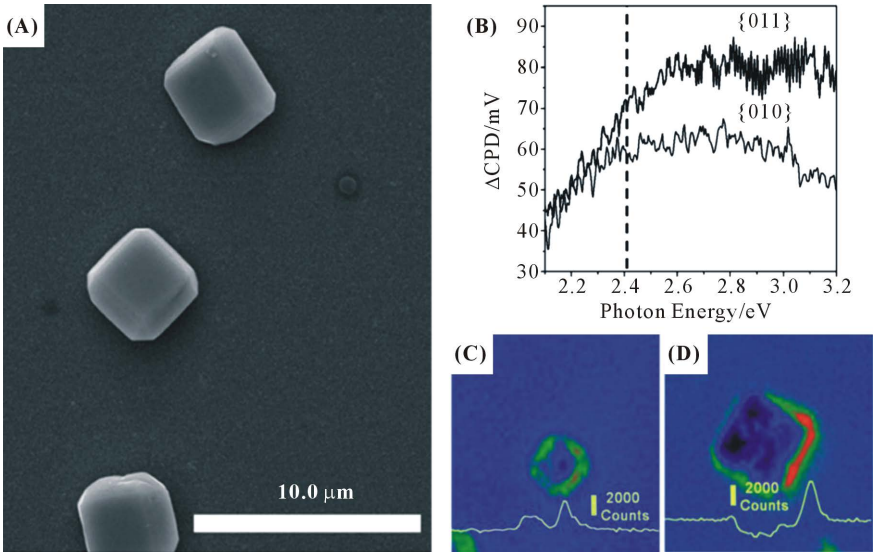

Figure 8. Direct imaging of highly anisotropic photogenerated charge separations on different facets of a single $BiVO_4$. (A) SEM images of single m-$BiVO_4$ crystals synthesized on FTO substrate. (B) Steady-state SPV spectroscopy of the {010} and {011} facets. (C) and (D) Fluorescence images of $BiVO_4$ particles on FTO substrate synthesized by different process in 5 mM APF solution, and its cross section with fluorescence intensity. Adapted with permission [36], copyright 2015, John Wiley and Sons.

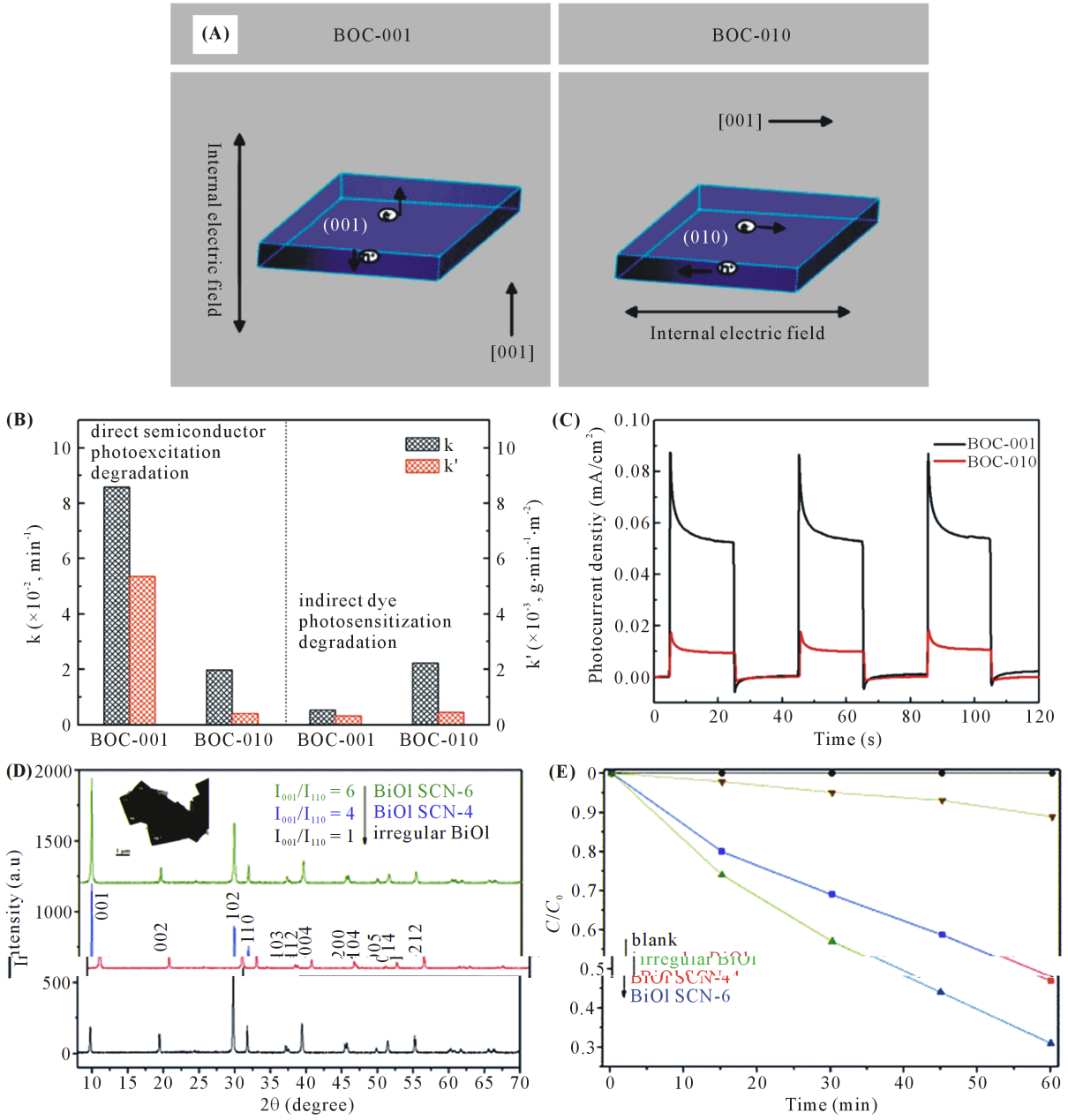

Figure 9. (A) Model showing the direction of the internal electric field in different oriented BiOCl single-crystal nanosheets (SCNSs) selectively synthesized via hydrothermal route. (B) Comparison of the apparent reaction rate constants for photocatalytic degradation of MO over different oriented BiOCl SCNSs under (left) UV (λ = 254 nm) and (right) visible-light (λ > 420 nm) irradiation. (C) Photocurrent responses of different oriented BiOCl SCNSs under UV-vis irradiation. Adapted with permission [40], copyright 2012, American Chemical Society. (D) XRD pattern and (E) corresponding photocatalytic testing of irregular BiOI and SCN with controlled {001} exposed facets percentage. Adapted with permission [51], copyright 2011, The Royal Society of Chemistry.

found that high photoactivity of {001} facets come from the high oxygen atoms density of {001} facets. Oxygen vacancies engender under UV light irradiation, which improve the separation efficiency of electrons and holes on surface. On the other hand, because of the internal electric field along the {001} direction caused by a $[Bi_2O_2]^{2+}$ cation layer and its adjacent halide layers, photo-induced electron-hole pairs separate along the {001} direction. According to the above mentioned reasons, {001} facet exposed BiOCl nanostructure, including nanosheets [42]-[44], porous nanoflowers [45] and nanodisk [46] have attract intensive attention. With the same

crystal structure and narrower band gap width, the same discipline applies to BiOBr and BiOI [47] (**Figure 9(D)**, **Figure 9(E)**). A series of BiOBr single crystal nanosheets, with the morphologies ranging from square nanoplates to thin lamellas were achieved in a hydrolysis system through adjusting temperature and solvent. With the increasing ratio of exposed {001} facets from 83% to 94%, the active photocatalysis in BiOBr crystals increases [48]. Hierarchical structures based on {001} faceted BiOBr or BiOI were also constructed [49]-[51]. Though a great deal of researches focus on the advantage of {001} facet exposed BiOX, nanosheets with same dominant {001} exposed facet were found to have different photoreactivity obtained from various hydrothermal pH value [52]. It's no coincidence that the size, surface area and surface state are still important factors in photocatalysis.

2.2.3. Titanium Dioxide (TiO_2)

Titanium dioxide (TiO_2) is one of the most extensive studied photocatalysts for environmental remediation and solar energy conversion through water splitting since the landmark set up by Fujishima and Honda in 1972 [1]. Recently, special attention has been paid on the facet-dependent property of TiO_2. Many studies revealed that crystals with different indices show various reactivity in photocatalysis [53] (**Figure 10(A)-(D)**). Generally, according to the Wulff construction [54], most available anatase TiO_2 crystals are dominated by thermodynamically stable {101} facets rather than {001} facets. The most abundant {101} facets of anatase were found to be not so reactive [55]. Inversely, the minority {001} surfaces show high reactivity indicated by the reconstruction under ultrahigh vacuum conditions [56]. Theoretical calculation also revealed the surface energies of anatase TiO_2 facets were in the order of 0.90 J/m^2 ({001}) > 0.53 J/m^2 ({100}) > 0.44 J/m^2 ({101}) [54]. In order to fabricate species with {001} facets exposed, novel crystal growth processes were explored. With the assistant of hydrofluoric acid as a morphology controlling agent, TiO_2 crystal with a high percentage of {001} facets can be synthesized [10]. Thenceforth vast reports demonstrated the synthesis of {001} facets exposed TiO_2 nanocrystals and TiO_2 based photocatalysts [57]-[59], and impressive photocatalytic performance were obtained.

However, practical situation seems more complex than expectation and contradictory opinion arise. Pan [60] synthesized a series of anatase TiO_2 with different percentages of {001}, {101} and {010} facets (**Figure 10(E)**). After photoreactivity comparison, they concluded that clean {001} exhibits lower reactivity than {101} in photooxidation reactions for hydrogen evolution. Furthermore, the {010} facets show the highest photoreactivity.

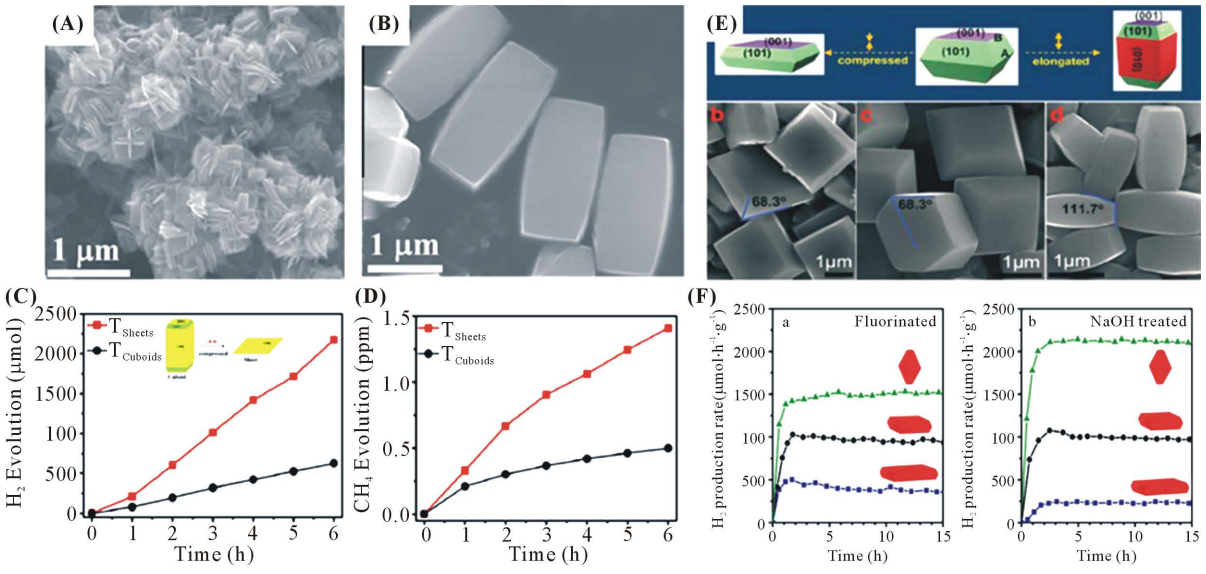

Figure 10. SEM image of the TiO_2 (A) nanosheets and (B) cuboids; comparison of (C) photocatalytic H_2 evolution tests of the 1 wt% Pt-loaded TiO_2 samples and (D) photocatalytic CO_2 photoreduction tests with different percentage of exposed {100} facets of the TiO_2 samples. Adapted with permission [53], copyright 2013, American Chemical Society. (E) Schematic of anatase TiO_2 crystals with different percentages of {101}, {001} and {010} facets, and corresponding SEM images of anatase crystals synthesized with different process parameters. Adapted with permission [60], copyright 2011, John Wiley and Sons. (F) Hydrogen production rate from 1 wt% Pt loaded samples of fluorinated and NaOH-treated TiO_2 NCs under solar illumination in 1:1 mixtures of MeOH/H_2O. Adapted with permission [61], copyright 2011, American Chemical Society.

This is also verified by Chen's work. [61] They compared the surface photocatalytic activity and the DSSC performance of {111}- and {010}-faceted anatase TiO_2, and confirmed that the performances are dependent on the crystal facet exposed, which increases in the order of non-facet < {111}-facet < {010}-facet. Different conclusions were reported by Zhang [62] [63]. By controlling the ratio of morphology controlling agent, they obtained {101}, {111}, and {001} facets exposed nanoscale anatase TiO_2 through hydrothermal route and calcined process. Their results revealed that {111} facets exhibit a better photocatalytic selective ability than {001} and {101} facets.

Interestingly, besides focusing attention on the order of different facets, synergy effect of low-energy facet and high-energy facet for enhanced photocatalysis was also employed. Roy [15] demonstrated that the presence of both the high-energy {001} oxidative and low-energy {101} reductive facets in an optimum ratio is necessary to reduce the charge recombination and thereby enhance photocatalytic activity of TiO_2 NCs. Murray`s preliminary experiments on the photoreforming of methanol on platinized samples, resulting in high volumes of evolved hydrogen under simulated solar illumination, suggested that the {101} facets of anatase are more active than the {001} (**Figure 10(F)**) [64]. This is due to the spontaneous separation of charge carriers and preferential flow of photogenerated carriers to the specific facets. The same mechanism was also supposed by Jiang [65]. The coexistence of adjacent facets with proper arrangement of band structures is benefit for the separation of photo-induced electron-hole pairs. This anisotropic transport properties leads to a lower recombination of photogenerated carriers and results in improvement of photocatalytic performance.

Most recently, several superduper reviews summarized the morphology control and anisotropic photocatalytic property, namely facet-dependent performance [3] [6] [9] [55] [66] of anatase TiO_2. The fabrication and application of special facets exposed TiO_2 were discussed systematically. Yet until now, the intrinsic mechanism for anisotropic photocatalytic property has no further discussion other than surface properties.

2.2.4. Cu_2O

Cuprous oxide (Cu_2O) is a nonstoichiometric p-type semiconductor with direct band gap of 2.17 eV, and is widely used as multifunctional material in field of solar energy conversion and solar-driven water splitting, gas sensors, and negative electrode material for lithium-ion batteries.

Shape-controlled synthesis of Cu_2O crystals has been attracting much interest due to the quite different active of exposed facets, and Cu_2O crystals with various exposed facets have been successfully synthesized. Sun [67] systematically investigated the crystal-facet-dependent effect of polyhedral Cu_2O microcrystals exposed with different-index facets on photocatalysis, and concluded that photocatalytic performance can be enhanced by high-index facets tailoring. Their results revealed that through elaborately controlling the synergistic effect of aggregation and ripening mechanism in crystal nucleation and growth process, 50-facet polyhedral Cu_2O with high-index {522} facets exhibited the highest activity in photo-degradation of the MO aqueous solution under UV irritation. They contributed it to the introduction of highly active components of high-index surfaces, which can offer more amount of unsaturated "Cu" dangling bonds and surface oxygen vacancies, and accelerate the formation of highly oxidative OH radicals.

Ho [68] synthesized cubic, truncated cubic, cuboctahedral, truncated octahedral, octahedral and short hexapod Cu_2O by a room temperature procedure. Octahedral Cu_2O with {111} facets showed higher photocatalytic activity than that of cubic Cu_2O with only {100} facets. Furthermore, extended hexapods Cu_2O with more {111} facets were more effective. However, reported by the same group [69], the rhombic dodecahedra exposing only the {110} facets exhibited even better photocatalytic activity than {111} faceted Cu_2O due to high number density of surface unsaturated copper atoms. The surface physicochemical property seems crucial in anisotropic photocatalysis. The facet-dependent activity was also utilized combined with surface plasmon resonance of Au core in polyhedral Au-Cu_2O core-shell nanocrystals [70].

On the other hand, noble metal decorations are usually used to improve the separation of photo-induced electron-hole pairs because of the Schottky barrier deriving from the arrangement of work function between semiconductor and metal. Wang [71] designed a Cu_2O-Pd hybrid structure to improve photocatalysis. Beside selective photo-reduce deposition of Pd on {100} as a result of charge spatial separation, however, difference of establishment of Schottky barrier between surface facets of Cu_2O was also noticed (**Figure 11**). In fact, not all the surface facets of Cu_2O polyhedron can offer appropriate work function to form Schottky barrier with Pd because of the various electronic structure. Potential analysis showed that the work function of Cu_2O {100} is much higher than {111} facet and more compatible with that of Pd. By selectively deposited Pd on the {111} facets of

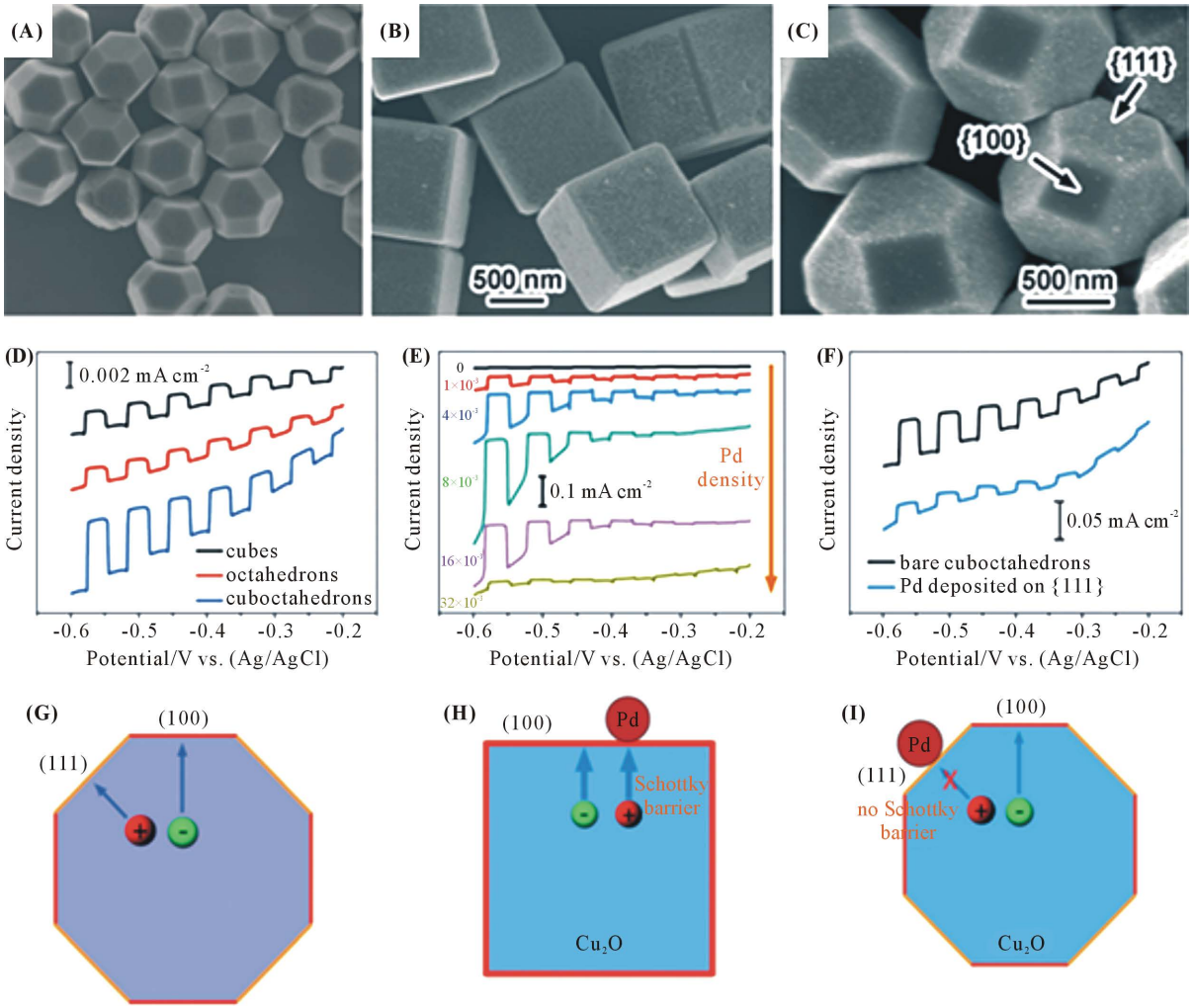

Figure 11. SEM images of (A) Cu_2O cuboctahedrons microcrystals; (B) Cu_2O cubes deposited with Pd and (C) Cu_2O cuboctahedrons with {111} facets selectively deposited with Pd. Photocurrent versus potential responses of photoelectrodes made of (D) different facet-exposed Cu_2O microsrystal, (E) Cu_2O cubes deposited with different amounts of Pd at the same Cu_2O loading weight, and (F) bare Cu_2O cuboctahedrons and those with {111} surface selectively deposited with Pd, respectively. Illustration of the charge spatial distribution and transfer in (G) bare Cu_2O cuboctahedrons. (H) Pd-decorated Cu_2O cubes; and (I) Pd deposited Cu_2O cuboctahedrons. Reproduced by permission [67], copyright 2014, John Wiley and Sons.

Cu_2O cuboctahedrons, the photocurrent was suppressed. In contrast, the photocurrent of Cu_2O cubes was significantly enhanced by addition of Pd nanoparticles on their {100} facets, and impressive efficiency was achieved by well-designed {100}-faceted Cu_2O cube decorated with Pd.

3. The Possibility to Tailoring the Effective Mass of Carriers

The anisotropic photocatalystic properties is one of the fatal factors that restrict the performance of nanostructured photocatalysts from more efficiency, for the prepared specimens are usually integration of both active facets and inactive facets, and even the latter maintain the dominant position. On the other hand, the anisotropy also provide the opportunity for further improving the performance by control the morphology with the most active facets exposed. Morphology controlling technology is regarded as a promising process in searching high-efficient photocatalysts, and now is one of the most interested research highlights in field of photocatalysis. However, high-reactive facets, usually the facets with high surface energy, degenerate and disappear during crystal growth in the solution-based synthesis process due to the thermodynamic stability. This makes the fabri-

cation of crystals exposed with high-reactive facets difficult. Additionally, synergy effect of low-energy and high-energy crystal facets for enhanced photocatalysis were also noticed over several photocatalysts [15]. Crystal with suitable proportion of low-energy and high-energy facets inhibit better performance than that with high-energy facets single. It seems that the synergistic effects of exposed facet play a larger role in photocatalysis than surface property and adsorption [15] [72].

Theoretical studies about charge carriers' properties, especially the effective masses of carriers in photocatalysts, were conducive to get a deeper insight over anisotropic photocatalytic properties. Calculation results based on density function theory help to explain the difference of photocatalytic property among ZnO, TiO_2 with different phases and AgX with different halogen successfully [16] [17] [73]. Moreover, theoretical prediction of the anisotropy of effective mass fit well with the experimental order of exposed facet activity. Effective mass is considered to be closely related to the transport and recombination of carriers. Modulation of the transport property and suppression of carriers' recombination is of vital important in photocatalysis, and is a promising method for improving the photocatalytic performance. State of the art, few attempts was carried out to tune the effective mass of charge carriers, which attribute to the reason that effective mass of carriers is determined by the gradient of band energy at *k* point. Graphically, the character of bonding orbital originate from correlated atom affect the effective mass and anisotropy of carriers. For example, *s* state is isotropous and beneficial of decreasing the effective mass, while *d* state deteriorate effective mass due to the localized feature. However, adjusting the compositions of energy band is much more difficult than tuning the width of bandgap. Introduction of exotic atom into lattice seems efficient for band engineering. Replace the lattice oxygen in ZnO with C, N and S, the effective masses of holes can be tuned, and leave the electrons effective masses near unchanged [74]. The same mechanism was proposed in N-S co-doped anatase TiO_2 [75]. Heteroatoms in lattice contribute to the band and change the DOS near Fermi level [74]. However, the mechanism seems much more complex than simply a mechanical mixture of electronic properties of both heteroatoms and pristine lattices' atoms [76]. WS_2 is a newly found photocatalyst with full solar light spectrum responsive capability [77]. By alloying with Mo, another star candidate in two dimensional transition-metal dichalcogenide family for photocatalyst [78], the resulting dichalcogenide alloys ($W_xMo_{1-x}S_2$) show composition-dependent electronic properties [79]. Based on first-principles calculations, it was found that effective mass of hole decreases linearly with increasing W composition, and effective mass of electron is always larger than that of their binary constituents, with the neglecting change of bandgap width [80]. The different behaviors of electrons and holes in alloys are attributed to the fact that metal *d* orbitals have different contributions to conduction bands of MoS_2 and WS_2, but almost identical contributions to valence bands. By modulation of the band structure, the carriers' property, including the effective mass and the mobility can be tuned since the latter is closely related to the former.

4. Summary and Prospect

Photocatalysis for environmental remediation and splitting water for generation of oxygen and/or hydrogen has become one of the most attractive fields for material scientists. Over the past decades, tremendous efforts have been devoted to morphology controlling of photocatalysts by elaborately adjustment of growth process, because the different efficiencies emerge from the fact that different exposed facets show various photocatalytic activity. With optimized exposed facets, the photocatalytic properties can be tremendous enhanced without any other modification of photocatalysts. Though great successes have been achieved, the underlying mechanisms are still unclear thoroughly. The investigation of charge carriers' properties brings us new perspective and method for a deeper insight of anisotropic photocatalytic property. The effective masses of carriers dramatically influenced the transport and recombination during photocatalysis, and the difference along various directions affects the activity on different facets, which fit well the nature of anisotropy of photocatalysts. Furthermore, the effective masses of carriers are decided by the structures of conduction band and valence band. The features of the orbitals that contribute to the conduction band and valence band determine the localization and directionality of the charge distribution between lattice atoms, resulting in the anisotropy of the carriers' effective masses. Theoretical calculations reveal that the impacts of *s* state, *p* state and *d* state on the effective masses distinguish apparently, and introduction of exotic atoms can obviously change the density of state near the Fermi level, which affects the effective masses. At this point, doping and solid solution treatments are promising in improving photocatalytic properties through modulation of effective masses of carriers and utilization of anisotropy of photocatalytic properties.

Acknowledgements

This work was supported by the National Natural Science Foundation of China (No. 51272121, 51221291, 51328203, and 51025205).

References

[1] Fujishima, A. and Honda, K. (1972) Electrochemical Photolysis of Water at a Semiconductor Electrode. *Nature*, **238**, 37-38. http://dx.doi.org/10.1038/238037a0

[2] Tong, H., *et al.* (2012) Nano-Photocatalytic Materials: Possibilities and Challenges. *Advanced Materials*, **24**, 229-251. http://dx.doi.org/10.1002/adma.201102752

[3] Dozzi, M. and Selli, E. (2013) Specific Facets-Dominated Anatase TiO_2: Fluorine-Mediated Synthesis and Photoactivity. *Catalysts*, **3**, 455-485. http://dx.doi.org/10.3390/catal3020455

[4] Sun, S. and Yang, Z. (2014) Recent Advances in Tuning Crystal Facets of Polyhedral Cuprous Oxide Architectures. *RSC Advances*, **4**, 3804-3822. http://dx.doi.org/10.1039/C3RA45445B

[5] Kuo, C.H. and Huang, M.H. (2010) Morphologically Controlled Synthesis of Cu_2O Nanocrystals and Their Properties. *Nano Today*, **5**, 106-116. http://dx.doi.org/10.1016/j.nantod.2010.02.001

[6] Ong, W.J., Tan, L.L., Chai, S.P., Yong, S.T. and Mohamed, A.R. (2014) Facet-Dependent Photocatalytic Properties of TiO_2-Based Composites for Energy Conversion and Environmental Remediation. *ChemSusChem*, **7**, 690-719. http://dx.doi.org/10.1002/cssc.201300924

[7] Huang, M.H., Rej, S. and Chiu, C.Y. (2015) Facet-Dependent Optical Properties Revealed through Investigation of Polyhedral Au-Cu_2O and Bimetallic Core-Shell Nanocrystals. *Small*, **11**, 2716-2726. http://dx.doi.org/10.1002/smll.201403542

[8] Martin, D.J., *et al.* (2015) Efficient Visible Driven Photocatalyst, Silver Phosphate: Performance, Understanding and Perspective. *Chemical Society Reviews*, **44**, 7808-7828. http://dx.doi.org/10.1039/C5CS00380F

[9] Ong, W.J., Tan, L.L., Chai, S.P., Yong, S.T. and Mohamed, A.R. (2014) Highly Reactive {001} Facets of TiO_2-Based Composites: Synthesis, Formation Mechanism and Characterization. *Nanoscale*, **6**, 1946-2008. http://dx.doi.org/10.1039/c3nr04655a

[10] Yang, H.G., *et al.* (2008) Anatase TiO_2 Single Crystals with a Large Percentage of Reactive Facets. *Nature*, **453**, 638-641. http://dx.doi.org/10.1038/nature06964

[11] Martin, D.J., Umezawa, N., Chen, X., Ye, J. and Tang, J. (2013) Facet Engineered Ag_3PO_4 for Efficient Water Photooxidation. *Energy & Environmental Science*, **6**, 3380-3386. http://dx.doi.org/10.1039/c3ee42260g

[12] Umezawa, N., Shuxin, O. and Ye, J. (2011) Theoretical Study of High Photocatalytic Performance of Ag_3PO_4. *Physical Review B*, **83**, Article ID: 035202. http://dx.doi.org/10.1103/PhysRevB.83.035202

[13] Wang, G., *et al.* (2012) Controlled Synthesis of Ag_2O Microcrystals with Facet-Dependent Photocatalytic Activities. *Journal of Materials Chemistry*, **22**, 21189-21194. http://dx.doi.org/10.1039/c2jm35010f

[14] Ma, X., Dai, Y., Guo, M. and Huang, B. (2013) Relative Photooxidation and Photoreduction Activities of the {100}, {101}, and {001} Surfaces of Anatase TiO_2. *Langmuir*, **29**, 13647-13654. http://dx.doi.org/10.1021/la403351v

[15] Roy, N., Sohn, Y. and Pradhan, D. (2013) Synergy of Low-Energy {101} and High-Energy {001} TiO_2 Crystal Facets for Enhanced Photocatalysis. *ACS Nano*, **7**, 2532-2540. http://dx.doi.org/10.1021/nn305877v

[16] Zhang, J., Zhou, P., Liu, J. and Yu, J. (2014) New Understanding of the Difference of Photocatalytic Activity among Anatase, Rutile and Brookite TiO_2. *Physical Chemistry Chemical Physics*, **16**, 20382-20386. http://dx.doi.org/10.1039/C4CP02201G

[17] Ma, X., Dai, Y., Guo, M. and Huang, B. (2012) The Role of Effective Mass of Carrier in the Photocatalytic Behavior of Silver Halide-Based Ag@AgX (X = Cl, Br, I): A Theoretical Study. *ChemPhysChem*, **13**, 2304-2309. http://dx.doi.org/10.1002/cphc.201200159

[18] Liu, J., Chen, S. and Zhu, Y. (2012) Electronic Structures and Effective Masses of Photogenerated Carriers of $CaZrTi_2O_7$ Photocatalyst: First-Principles Calculations. *Solid State Communications*, **152**, 1650-1654. http://dx.doi.org/10.1016/j.ssc.2012.05.004

[19] Zhao, Z., Li, Z. and Zou, Z. (2011) Electronic Structure and Optical Properties of Monoclinic Clinobisvanite $BiVO_4$. *Physical Chemistry Chemical Physics*, **13**, 4746-4753. http://dx.doi.org/10.1039/c0cp01871f

[20] Yan, S., *et al.* (2013) An Ion-Exchange Phase Transformation to $ZnGa_2O_4$ Nanocube towards Efficient Solar Fuel Synthesis. *Advanced Functional Materials*, **23**, 758-763. http://dx.doi.org/10.1002/adfm.201202042

[21] Li, Z., *et al.* (2014) Tuning Photocatalytic Performance of the Near-Infrared-Driven Photocatalyst $Cu_2(OH)PO_4$ Based

on Effective Mass and Dipole Moment. *Physical Chemistry Chemical Physics*, **16**, 3267-3273. http://dx.doi.org/10.1039/c3cp53381f

[22] Bi, Y., *et al.* (2012) Photocatalytic and Photoelectric Properties of Cubic Ag_3PO_4 Sub-Microcrystals with Sharp Corners and Edges. *Chemical Communications*, **48**, 3748-3750. http://dx.doi.org/10.1039/c2cc30363a

[23] Bi, Y., Hu, H.Y., Ouyang, S.X., Jiao, Z.B., Lu, G.X. and Ye, J.H. (2012) Selective Growth of Metallic Ag Nanocrystals on Ag_3PO_4 Submicro-Cubes for Photocatalytic Applications. *Chemistry*, **18**, 14272-14275. http://dx.doi.org/10.1002/chem.201201435

[24] Bi, Y., Ouyang, S., Umezawa, N., Cao, J. and Ye, J.H. (2011) Facet Effect of Single-Crystalline Ag_3PO_4 Sub-Microcrystals on Photocatalytic Properties. *Journal of the American Chemical Society*, **133**, 6490-6492. http://dx.doi.org/10.1021/ja2002132

[25] Wang, H., *et al.* (2012) Facile Synthesis of Ag_3PO_4 Tetrapod Microcrystals with an Increased Percentage of Exposed {110} Facets and Highly Efficient Photocatalytic Properties. *CrystEngComm*, **14**, 8342-8344. http://dx.doi.org/10.1039/c2ce26366a

[26] Wang, J., *et al.* (2013) Facile Synthesis of Novel Ag_3PO_4 Tetrapods and the {110} Facets-Dominated Photocatalytic Activity. *CrystEngComm*, **15**, 39-42. http://dx.doi.org/10.1039/C2CE26060C

[27] Jiao, Z.B., *et al.* (2013) Concave Trisoctahedral Ag_3PO_4 Microcrystals with High-Index Facets and Enhanced Photocatalytic Properties. *Chemical Communications*, **49**, 636-638. http://dx.doi.org/10.1039/C2CC37324F

[28] Wang, H., *et al.* (2012) Facet-Dependent Photocatalytic Properties of AgBr Nanocrystals. *Small*, **8**, 2802-2806. http://dx.doi.org/10.1002/smll.201200055

[29] Wang, H., *et al.* (2012) Facile Synthesis of AgBr Nanoplates with Exposed {111} Facets and Enhanced Photocatalytic Properties. *Chemical Communications*, **48**, 275-277. http://dx.doi.org/10.1039/C1CC16423F

[30] Zhang, H., Lu, Y., Liu, H. and Fang, J. (2015) One-Pot Synthesis of High-Index Faceted AgCl Nanocrystals with Trapezohedral, Concave Hexoctahedral Structures and Their Photocatalytic Activity. *Nanoscale*, **7**, 11591-11601. http://dx.doi.org/10.1039/C5NR02049B

[31] Wang, H., *et al.* (2012) Polyhedral AgBr Microcrystals with an Increased Percentage of Exposed {111} Facets as a Highly Efficient Visible-Light Photocatalyst. *Chemistry*, **18**, 4620-4626. http://dx.doi.org/10.1002/chem.201102694

[32] Kuang, Q., Zheng, X. and Yang, S. (2014) AgI Microplate Monocrystals with Polar {0001} Facets: Spontaneous Photocarrier Separation and Enhanced Photocatalytic Activity. *Chemistry*, **20**, 2637-2645. http://dx.doi.org/10.1002/chem.201303642

[33] Li, R., *et al.* (2013) Spatial Separation of Photogenerated Electrons and Holes among {010} and {110} Crystal Facets of $BiVO_4$. *Nature Communications*, **4**, Article No. 1432. http://dx.doi.org/10.1038/ncomms2401

[34] Li, R., Han, H., Zhang, F., Wang, D. and Li, C. (2014) Highly Efficient Photocatalysts Constructed by Rational Assembly of Dual-Cocatalysts Separately on Different Facets of $BiVO_4$. *Energy & Environmental Science*, **7**, 1369-1376. http://dx.doi.org/10.1039/c3ee43304h

[35] Liu, T., Zhou, X., Dupuisc, M. and Li, C. (2015) The Nature of Photogenerated Charge Separation among Different Crystal Facets of $BiVO_4$. *Physical Chemistry Chemical Physics*, **17**, 23503-23510. http://dx.doi.org/10.1039/C5CP04299B

[36] Zhu, J., *et al.* (2015) Direct Imaging of Highly Anisotropic Photogenerated Charge Separations on Different Facets of a Single $BiVO_4$ Photocatalyst. *Angewandte Chemie International Edition*, **54**, 9111-9114. http://dx.doi.org/10.1002/anie.201504135

[37] Wang, D., *et al.* (2011) Crystal Facet Dependence of Water Oxidation on $BiVO_4$ Sheets under Visible Light Irradiation. *Chemistry*, **17**, 1275-1282. http://dx.doi.org/10.1002/chem.201001636

[38] Xi, G. and Ye, J.H. (2010) Synthesis of Bismuth Vanadate Nanoplates with Exposed {001} Facets and Enhanced Visible-Light Photocatalytic Properties. *Chemical Communications*, **46**, 1893-1895. http://dx.doi.org/10.1039/b923435g

[39] Thalluri, S.M., *et al.* (2014) Green-Synthesized $BiVO_4$ Oriented along {040} Facets for Visible-Light-Driven Ethylene Degradation. *Industrial & Engineering Chemistry Research*, **53**, 2640-2646. http://dx.doi.org/10.1021/ie403999g

[40] Jiang, J., Zhao, K., Xiao, X. and Zhang, L. (2012) Synthesis and Facet-Dependent Photoreactivity of BiOCl Single-Crystalline Nanosheets. *Journal of the American Chemical Society*, **134**, 4473-4476. http://dx.doi.org/10.1021/ja210484t

[41] Ye, L., Zan, L., Tian, L., Peng, T. and Zhang, J. (2011) The {001} Facets-Dependent High Photoactivity of BiOCl Nanosheets. *Chemical Communications*, **47**, 6951-6953. http://dx.doi.org/10.1039/c1cc11015b

[42] Cui, Z., Mi, L. and Zeng, D. (2013) Oriented Attachment Growth of BiOCl Nanosheets with Exposed {110} Facets and Photocatalytic Activity of the Hierarchical Nanostructures. *Journal of Alloys and Compounds*, **549**, 70-76. http://dx.doi.org/10.1016/j.jallcom.2012.09.075

[43] Peng, Y., Wang, D., Zhou, H.Y. and Xu, A.W. (2015) Controlled Synthesis of Thin BiOCl Nanosheets with Exposed {001} Facets and Enhanced Photocatalytic Activities. *CrystEngComm*, **17**, 3845-3851. http://dx.doi.org/10.1039/C5CE00289C

[44] Li, Y., Wang, Q., Liu, B. and Zhang, J. (2015) The {001} Facets-Dependent Superior Photocatalytic Activities of Bi-OCl Nanosheets under Visible Light Irradiation. *Applied Surface Science*, **349**, 957-969. http://dx.doi.org/10.1016/j.apsusc.2015.05.100

[45] Wang, D. H., *et al.* (2012) Nanosheet-Constructed Porous BiOCl with Dominant {001} Facets for Superior Photosensitized Degradation. *Nanoscale*, **4**, 7780-7785. http://dx.doi.org/10.1039/c2nr32533k

[46] Zhang, X., *et al.* (2014) Synthesis of a Highly Efficient BiOCl Single-Crystal Nanodisk Photocatalyst with Exposing {001} Facets. *ACS Applied Materials & Interfaces*, **6**, 7766-7772. http://dx.doi.org/10.1021/am5010392

[47] Ye, L., Su, Y., Jin, X., Xie, H. and Zhang, C. (2014) Recent Advances in BiOX (X = Cl, Br and I) Photocatalysts: Synthesis, Modification, Facet Effects and Mechanisms. *Environmental Science*: *Nano*, **1**, 90-112. http://dx.doi.org/10.1039/c3en00098b

[48] Zhang, D., Li, J., Wang, Q. and Wu, Q. (2013) High {001} Facets Dominated BiOBr Lamellas: Facile Hydrolysis Preparation and Selective Visible-Light Photocatalytic Activity. *Journal of Materials Chemistry A*, **1**, 8622-8629. http://dx.doi.org/10.1039/c3ta11390f

[49] Ye, L., Liu, J., Jiang, Z., Peng, T. and Zan, L. (2013) Facets Coupling of BiOBr-g-C_3N_4 Composite Photocatalyst for Enhanced Visible-Light-Driven Photocatalytic Activity. *Applied Catalysis B*: *Environmental*, **142-143**, 1-7. http://dx.doi.org/10.1016/j.apcatb.2013.04.058

[50] Sun, L., *et al.* (2015) Enhanced Visible-Light Photocatalytic Activity of BiOI/BiOCl Heterojunctions: Key Role of Crystal Facet Combination. *ACS Catalysis*, **5**, 3540-3551. http://dx.doi.org/10.1021/cs501631n

[51] Ye, L., Tian, L., Peng, T. and Zan, L. (2011) Synthesis of Highly Symmetrical BiOI Single-Crystal Nanosheets and Their {001} Facet-Dependent Photoactivity. *Journal of Materials Chemistry*, **21**, 12479-12484. http://dx.doi.org/10.1039/c1jm11005e

[52] Ye, L., Su, Y.R., Jin, X.L., Xie, H.Q., Cao, F.P. and Guo, Z. (2014) Which Affect the Photoreactivity of BiOBr Single-Crystalline Nanosheets with Different Hydrothermal pH Value: Size or Facet? *Applied Surface Science*, **311**, 858-863.

[53] Xu, H., Ouyang, S.X., Li, P., Kako, T. and Ye, J.H. (2013) High-Active Anatase TiO_2 Nanosheets Exposed with 95% {100} Facets toward Efficient H_2 Evolution and CO_2 Photoreduction. *ACS Applied Materials & Interfaces*, **5**, 1348-1354. http://dx.doi.org/10.1021/am302631b

[54] Lazzeri, M., Vittadini, A. and Selloni, A. (2001) Structure and Energetics of Stoichiometric TiO_2 Anatase Surfaces. *Physical Review B*, **63**, Article ID: 155409. http://dx.doi.org/10.1103/PhysRevB.63.155409

[55] Selloni, A. (2008) Anatase Shows Its Reactive Side. *Nature Materials*, **7**, 613-615. http://dx.doi.org/10.1038/nmat2241

[56] Herman, G.S., Sievers, M.R. and Gao, Y. (2000) Structure Determination of the Two-Domain (1 × 4) Anatase TiO_2 (001) Surface. *Physical Review Letters*, **84**, 3354-3357. http://dx.doi.org/10.1103/PhysRevLett.84.3354

[57] Sun, L., Zhao, Z., Zhou, Y. and Liu, L. (2012) Anatase TiO_2 Nanocrystals with Exposed {001} Facets on Graphene Sheets via Molecular Grafting for Enhanced Photocatalytic Activity. *Nanoscale*, **4**, 613-620. http://dx.doi.org/10.1039/C1NR11411E

[58] Liu, S., Yu, J. and Jaroniec, M. (2011) Anatase TiO_2 with Dominant High-Energy {001} Facets: Synthesis, Properties, and Applications. *Chemistry of Materials*, **23**, 4085-4093. http://dx.doi.org/10.1021/cm200597m

[59] Xu, H., *et al.* (2013) Anatase TiO_2 Single Crystals Exposed with High-Reactive {111} Facets toward Efficient H_2 Evolution. *Chemistry of Materials*, **25**, 405-411. http://dx.doi.org/10.1021/cm303502b

[60] Pan, J., Liu, G., Lu, G.Q. and Cheng, H.M. (2011) On the True Photoreactivity Order of {001}, {010}, and {101} Facets of Anatase TiO_2 Crystals. *Angewandte Chemie International Edition*, **50**, 2133-2137. http://dx.doi.org/10.1002/anie.201006057

[61] Chen, C.D., *et al.* (2015) Synthesis of [111]- and {010}-Faceted Anatase TiO_2 Nanocrystals from Tri-Titanate Nanosheets and Their Photocatalytic and DSSC Performances. *Nanoscale*, **7**, 7980-7991. http://dx.doi.org/10.1039/C5NR00069F

[62] Zhang, J., *et al.* (2014) Nanoscale Anatase TiO_2 with Dominant {111} Facets Shows High Photocatalytic Activity. *Applied Surface Science*, **311**, 521-528. http://dx.doi.org/10.1016/j.apsusc.2014.05.103

[63] Zhang, J., *et al.* (2014) Regulating Photocatalytic Selectivity of Anatase TiO_2 with {101}, {001}, and {111} Facets. *Journal of the American Ceramic Society*, **97**, 4005-4010. http://dx.doi.org/10.1111/jace.13187

[64] Gordon, T.R., *et al.* (2012) Nonaqueous Synthesis of TiO_2 Nanocrystals Using TiF_4 to Engineer Morphology, Oxygen Vacancy Concentration, and Photocatalytic Activity. *Journal of the American Chemical Society*, **134**, 6751-6761. http://dx.doi.org/10.1021/ja300823a

[65] Jiang, G.D., Wei, M., Yuan, S.D. and Chang, Q. (2016) Efficient Photocatalytic Reductive Dechlorination of 4-Chlorophenolto Phenol on {001}/{101} Facets Co-Exposed TiO_2 Nanocrystals. *Applied Surface Science*, **362**, 418-426. http://dx.doi.org/10.1016/j.apsusc.2015.11.229

[66] Grabowska, E., Diak, M., Marchelek, M. and Zaleska, A. (2014) Decahedral TiO_2 with Exposed Facets: Synthesis, Properties, Photoactivity and Applications. *Applied Catalysis B*: *Environmental*, **156-157**, 213-235. http://dx.doi.org/10.1016/j.apcatb.2014.03.019

[67] Sun, S., Song, X., Sun, Y., Deng, D. and Yang, Z. (2012) The Crystal-Facet-Dependent Effect of Polyhedral Cu_2O Microcrystals on Photocatalytic Activity. *Catalysis Science & Technology*, **2**, 925-930. http://dx.doi.org/10.1039/c2cy00530a

[68] Ho, J.Y. and Huang, M.H. (2009) Synthesis of Submicrometer-Sized Cu_2O Crystals with Morphological Evolution from Cubic to Hexapod Structures and Their Comparative Photocatalytic Activity. *Journal of Physical Chemistry C*, **113**, 14159-14164. http://dx.doi.org/10.1021/jp903928p

[69] Huang, W.C., Lyu, L.M., Yang, Y.C. and Huang, M.H. (2012) Synthesis of Cu_2O Nanocrystals from Cubic to Rhombic Dodecahedral Structures and Their Comparative Photocatalytic Activity. *Journal of the American Chemical Society*, **134**, 1261-1267. http://dx.doi.org/10.1021/ja209662v

[70] Yang, Y.C., *et al.* (2014) Facet-Dependent Optical Properties of Polyhedral Au-Cu_2O Core-Shell Nanocrystals. *Nanoscale*, **6**, 4316-4324. http://dx.doi.org/10.1039/c3nr06293g

[71] Wang, L., *et al.* (2014) Designing p-Type Semiconductor-Metal Hybrid Structures for Improved Photocatalysis. *Angewandte Chemie International Edition*, **53**, 5107-5111.

[72] Xing, M., *et al.* (2013) Enhanced Photocatalysis by Au Nanoparticle Loading on TiO_2 Single-Crystal (001) and (110) Facets. *The Journal of Physical Chemistry Letters*, **4**, 3910-3917.

[73] Dong, M., Zhang, J. and Yu, J. (2015) Effect of Effective Mass and Spontaneous Polarization on Photocatalytic Activity of Wurtzite and Zinc-Blende ZnS. *APL Materials*, **3**, Article ID: 104404. http://dx.doi.org/10.1063/1.4922860

[74] Yu, W., Zhang, J. and Peng, T. (2016) New Insight into the Enhanced Photocatalytic Activity of N-, C- and S-Doped ZnO Photocatalysts. *Applied Catalysis B*: *Environmental*, **181**, 220-227. http://dx.doi.org/10.1016/j.apcatb.2015.07.031

[75] Zhou, P., Yu, J. and Wang, Y. (2013) The New Understanding on Photocatalytic Mechanism of Visible-Light Response N-S Codoped Anatase TiO_2 by First-Principles. *Applied Catalysis B*: *Environmental*, **142-143**, 45-53. http://dx.doi.org/10.1016/j.apcatb.2013.04.063

[76] Yu, J., Zhou, P. and Li, Q. (2013) New Insight into the Enhanced Visible-Light Photocatalytic Activities of B-, C- and B/C-Doped Anatase TiO_2 by First-Principles. *Physical Chemistry Chemical Physics*, **15**, 12040-12047. http://dx.doi.org/10.1039/c3cp44651d

[77] Sang, Y., *et al.* (2015) From UV to Near-Infrared, WS_2 Nanosheet: A Novel Photocatalyst for Full Solar Light Spectrum Photodegradation. *Advanced Materials*, **27**, 363-369. http://dx.doi.org/10.1002/adma.201403264

[78] King, L.A., Zhao, W., Chhowalla, M., Riley, D.J. and Eda, G. (2013) Photoelectrochemical Properties of Chemically Exfoliated MoS_2. *Journal of Materials Chemistry A*, **1**, 8935-8941. http://dx.doi.org/10.1039/c3ta11633f

[79] Xi, J., Zhao, T., Wang, D. and Shuai, Z. (2014) Tunable Electronic Properties of Two-Dimensional Transition Metal Dichalcogenide Alloys: A First-Principles Prediction. *The Journal of Physical Chemistry Letters*, **5**, 285-291. http://dx.doi.org/10.1021/jz402375s

[80] Faraji, M., *et al.* (2015) Band Engineering and Charge Separation in the $Mo_{1-x}W_xS_2/TiO_2$ Heterostructure by Alloying: First Principle Prediction. *RSC Advances*, **5**, 28460-28466. http://dx.doi.org/10.1039/C5RA00330J